Bioconjugate Chemistry

Article

pubs.acs.org/bc

Conjugation of Antibodies to Gold Nanorods through Fc Portion: Synthesis and Molecular Specific Imaging

Pratixa P. Joshi,[†] Soon Joon Yoon,[†] William G. Hardin,[§] Stanislav Emelianov,[†,‡] and Konstantin V. Sokolov*[,†,‡]

[†]Department of Biomedical Engineering and [§]Texas Materials Institute, University of Texas at Austin, Austin, Texas 78712, United States

[‡]Department of Imaging Physics, M.D. Anderson Cancer Center, Houston, Texas 77030, United States

Supporting Information

ABSTRACT: Anisotropic gold nanorods provide a convenient combination of properties, such as tunability of plasmon resonances and strong extinction cross sections in the near-infrared to red spectral region. These properties have created significant interest in the development of antibody conjugation methods for synthesis of targeted nanorods for a number of biomedical applications, including molecular specific imaging and therapy. Previously published conjugation approaches have achieved molecular specificity. However, the current conjugation methods have several downsides including low stability and potential cytotoxicity of bioconjugates that are produced by electrostatic interactions, as well as lack of control over antibody orientation during covalent conjugation. Here we addressed these shortcomings by introducing directional antibody conjugation to the gold nanorod surface. The directional conjugation is achieved through the carbohydrate moiety, which is located on one of the heavy chains of the Fc portion of most antibodies. The carbohydrate is oxidized under mild conditions to a hydrazide reactive aldehyde group. Then, a heterofunctional linker with hydrazide and dithiol groups is used to attach antibodies to gold nanorods. The directional conjugation approach was characterized using electron microscopy, zeta potential, and extinction spectra. We also determined spectral changes associated with nanorod aggregation; these spectral changes can be used as a convenient quality control of nanorod bioconjugates. Molecular specificity of the synthesized antibody targeted nanorods was demonstrated using hyperspectral, optical and photoacoustic imaging of cancer cell culture models. Additionally, we observed characteristic changes in optical spectra of molecular specific nanorods after their interactions with cancer cells; the observed spectral signatures can be explored for sensitive cancer detection.

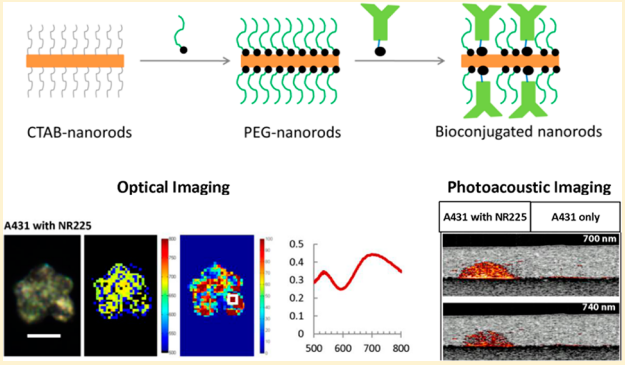

INTRODUCTION

Plasmonic gold nanoparticles have become an area of intense focus in biology and medicine due to their small size and intrinsic properties that offer the potential to solve otherwise intractable problems.[1−28] In general, plasmonic nanoparticles are intrinsically multimodal contrast agents since they exhibit strong scattering and absorption cross sections as well as nonlinear optical phenomena such as two-photon luminescence and second harmonic generation when excited at the plasmon resonance frequency. Gold nanoparticles provide high contrast in cellular and tissue imaging using confocal reflectance microscopy,[1,29] dark-field imaging,[7,29−32] two-photon luminescence,[33−35] phase-sensitive optical coherence tomography,[17] and photoacoustic imaging.[13,14,36−43] Furthermore, gold nanoparticles have been used to transform light energy into heat in photothermal therapy of cancer either by using near-IR (NIR) absorbing gold nanoshells,[3,5,44,45] nanorods,[10] and nanocages[15,46,47] or by applying molecular-targeted spherical nanoparticles which undergo molecular specific aggregation upon interaction with cancer cells that results in strong absorption in the red- to NIR-spectral region due to plasmon resonance coupling.[12,48] The use of NIR irradiation is essential for *in vivo* applications because NIR light has the best tissue penetration depth.[49,50] In more recent developments, gold nanoparticles have been explored as carriers of nucleic acids such as siRNA or antisense DNA molecules that can be selectively activated or released using light irradiation, which results in remotely triggered gene silencing.[51−53]

Among all available nanoparticle geometries anisotropic gold nanorods provide a convenient combination of properties for biomedical applications.[54−56] Plasmon resonances of gold nanorods can be easily tuned in the red-NIR spectral region by changing the nanorod aspect ratio[57] that allows simultaneous imaging of multiple biomarkers.[58,59] Strong NIR

Received: August 29, 2012
Revised: March 29, 2013
Published: April 30, 2013

   dx.doi.org/10.1021/bc3004815 | *Bioconjugate Chem.* 2013, 24, 878−888

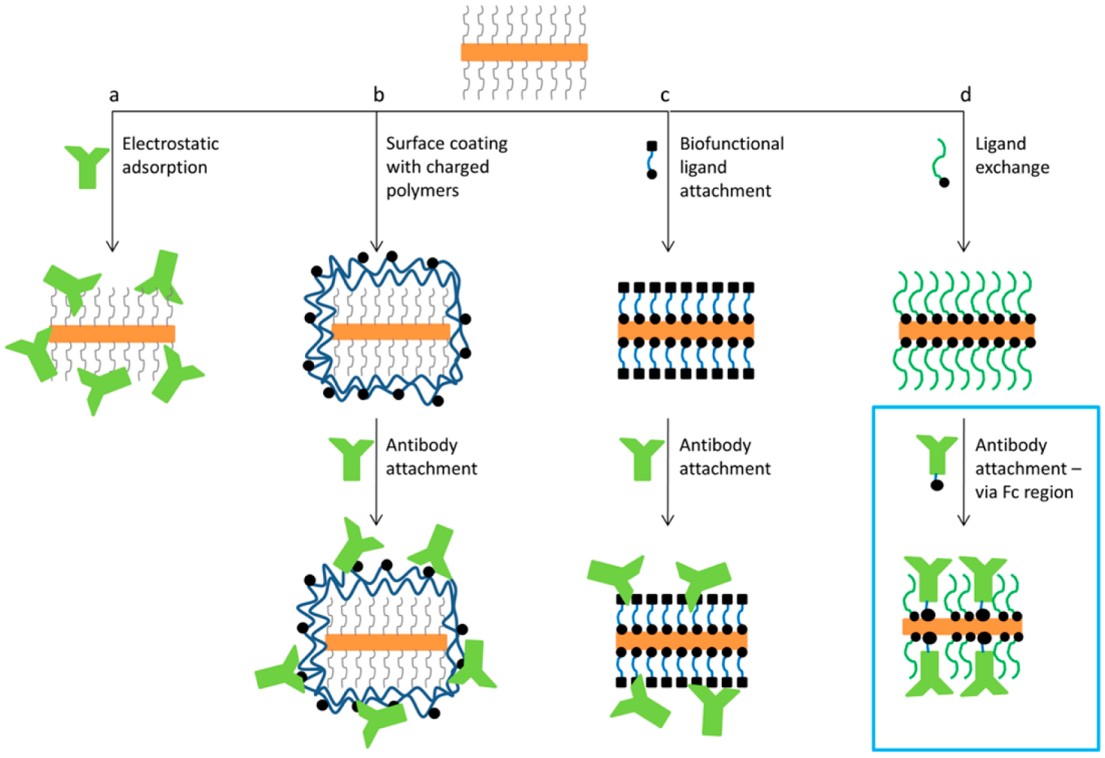

Figure 1. Schematic representation of gold nanorod bioconjugation procedures from left to right: electrostatic adsorption of antibodies to CTAB layer on gold nanorods; coating of CTAB nanorods by charged polymers followed by electrostatic adsorption of antibodies; replacement of the CTAB layer using bifunctional ligands followed by covalent attachment of antibodies; the directional conjugation method proposed here that consist of replacement of the CTAB layer with mPEG-thiol molecules followed by directional attachment of antibodies.

extinction cross sections of nanorods have been used for two-photon luminescence[33,34] and photoacoustic[60−62] imaging of thick biological samples as well as for photothermal destruction of cancer cells.[10,63,64] It was also observed that anisotropic arrangement of epidermal growth factor receptor (EGFR) targeted gold nanorods on the surface of cancer cells produces surface-enhanced Raman scattering that could be used as a marker of EGFR overexpressing cells.[65] Furthermore, the anisotropy property of nanorods has been explored for dynamic imaging of rotational motion in 3D space.[66]

Surface modification of nanoparticles is critical for both *in vitro* and *in vivo* applications, as uncoated nanoparticles are colloidally unstable and often cytotoxic in biological solutions.[67−70] Conjugation of biomolecules to nanoparticles furnishes important properties needed for biomedical applications, such as molecular targeting, stealth properties and surface charge. Antibodies are the most widely used targeting moieties due to their high affinity and availability for a large number of established biomarkers.

Conjugation to gold nanorods is confounded by the presence of surface layer of cetyl trimethyl ammonium bromide (CTAB). In commonly used synthesis of highly uniform gold nanorods the CTAB molecules promote crystal growth in one direction that results in rod-shaped particles.[71] CTAB layer on the gold surface is stabilized by electrostatic interactions between gold and CTAB as well as by hydrophobic interactions in a bilayer of CTAB molecules. A recent review by El-Sayed's group[54] summarizes current methods of nanorod bioconjugation: (1) electrostatic adsorption of biomolecules directly to the CTAB layer; (2) coating of CTAB layer with one or more layers of charged polymers followed by physisorption or covalent attachment of targeting moieties; (3) bifunctional ligand attachment where CTAB is first replaced by bifunctional linker molecules followed by conjugation of biomolecules; and (4) ligand exchange where CTAB is replaced by small thiolated molecules (Figure 1). Although these conjugation methods have been used to achieve molecular specificity, they have a number of major shortcomings which have to be addressed in order to further optimize gold nanorods for molecular specific imaging and therapy. In the first two approaches, the CTAB bilayer is still present on nanorods that can lead to long-term cytotoxicity of the bioconjugates.[72] In addition, the physisorption approach requires a high concentration of antibodies for synthesis of nanoparticle conjugates, results in random orientation of antibodies at the gold surface, and can be prone to antibody replacement by other molecules in biological samples.[73] In the third approach, the CTAB bilayer was first replaced by small bifunctional linkers with thiol functional groups for interaction with the gold surface and carboxyl groups for covalent attachment of antibodies using carbodiimide chemistry.[58,74,75] In this strategy, antibodies are attached through primary amine groups.[76,77] Because the primary amine groups are present in different portions of antibody molecules, including antigen recognition sites on the Fab region, this conjugation approach does not provide control over antibody orientation on the nanoparticle surface, leading to reduced activity of the attached antibodies. In addition, this conjugation strategy is prone to aggregation because antibody molecules have both the primary amine and the carboxyl groups, which can act as cross-linking agents between gold nanoparticles. The fourth approach has been used to produce nonspecific biocompatible nanorods by replacing the CTAB bilayer with biocompatible ligands such as polyethylene glycol (PEG).[78]

dx.doi.org/10.1021/bc3004815 | *Bioconjugate Chem.* 2013, 24, 878−888

Here we address the shortcomings of previously published conjugation protocols by developing directional attachment of antibodies to gold nanorods using a two-step method (Figure 1). First, the CTAB bilayer on nanorods is replaced with methoxy-poly(ethylene)glycol thiol (mPEG-SH). Then, thiolated antibody molecules are attached via Fc portion which does not have antibody binding sites using ligand exchange with mPEG-SH. The directional conjugation is achieved by specific reaction of the carbohydrate moiety located on the Fc portion of most antibodies with a heterofunctional cross-linker; this reaction results in antibodies with a dithiol group located in one specific position in the Fc region. The dithiol enables antibody conjugation directly to the gold surface. We showed that this method produces stable bioconjugates with no aggregation and no cytotoxicity. In addition, it requires a significantly reduced amount of antibodies during the synthesis as compared to physisorption methods. We also demonstrated that synthesized antibody gold nanorod conjugates can be used for molecular specific optical and photoacoustic imaging of epidermal growth factor receptor (EGFR) molecules in cancer cell culture models.

EXPERIMENTAL PROCEDURES

Gold Nanorod Synthesis. Gold nanorods were synthesized by seed mediated growth mechanism using the previously published protocol.[71] Briefly, 100 μL of 4 mM $AgNO_3$ (Acros Organics, 41936) was added to 10 mL of 0.5 mM $HAuCl_4$ (Sigma, 520918) dissolved in 0.1 M CTAB (Amresco, 0833) solution. Then, 70 μL of 78.8 mM ascorbic acid (Acros Organics, 401471000) was added to the reaction mixture as a mild reducing agent; this constitutes the nanorod growth solution. In parallel, a seed solution was prepared by mixing 0.6 mL of 10 mM ice-cold $NaBH_4$ (Fisher, S678) to 10 mL of 0.25 mM $HAuCl_4$ dissolved in 0.1 M CTAB solution. To initialize the growth of nanorods, 12 μL of the seed solution was added to the nanorod growth solution within 30 min of making the seed solution. Then, the reaction mixture was kept at 30 °C for at least 2 h for completion of nanorod synthesis. The nanorods were washed twice with water by centrifugation at 18 000 × g for 45 min. The final nanorod pellet was dispersed in water and stored at room temperature. Nanorods were 20× concentrated compared to the as-prepared nanorods.

Gold Nanorod Bioconjugation. The nanorods were bioconjugated in two steps (Figure 2). The first step involved replacement of the CTAB layer on nanorod surface with methoxy-PEG-thiol (mPEG-SH). One hundred microliters of 0.5 mM mPEG-SH with molecular weight 2000 Da (Creative PEGworks, PLS-605) were mixed with 1 mL of CTABNRs (20× concentrated compared to as-prepared nanorods) and sonicated using a water bath sonicator (Branson 1510R-MT) for 30 min at room temperature. After sonication, free CTAB and mPEG-SH molecules were removed by centrifugation using 100 KDa centrifugal filters at 2500 × g for 15 min. Then, the nanorods were washed one time with water to remove any residual mPEG and CTAB. The prepared mPEG-NRs were dispersed in 1 mL water and stored at room temperature.

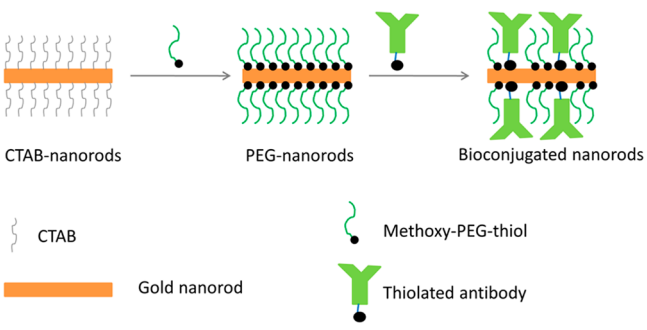

Figure 2. Schematic illustration of the directional conjugation synthesis proposed here.

In the second conjugation step, the carbohydrate moiety on Fc portion of anti-EGFR clone 225 (Sigma, E2156) or RG-16 (Sigma, I0138) antibodies were thiolated following our previously published protocol.[79] Briefly, antibodies were concentrated using 50 kDa MWCO centrifugal filter and were dissolved in 100 mM Na_2HPO_4, pH 7.5 buffer at 1 mg/mL. Then, 10 μL of 100 mM $NaIO_4$ in water was added to 100 μL of antibody solution and the mixture was incubated in dark for 30 min. The reaction was quenched by adding 500 μL of phosphate buffered saline (PBS). At this point the carbohydrate moieties on the Fc portion of the antibody were oxidized to aldehyde groups.[79,80] Then, 140-times molar excess of heterofunctional linker dithiolaromatic PEG6-CONHNH2 (SensoPath Technologies, SPT-0014B) was added to the antibody solution. The linker has hydrazide and dithiol groups on opposing sites of the molecule. The hydrazide moiety interacts with aldehyde groups of the Fc portion of the modified antibody molecules. The reaction mixture was incubated at room temperature for 1 h and then the thiolated antibodies were collected using centrifugal filters and resuspended in 0.1 M sodium phosphate buffer, pH 7.5. Two hundred microliters of the thiolated anti-EGFR antibodies at concentration of 1 mg/mL were mixed with 0.1 mL of mPEG-NRs and the suspension was incubated at room temperature for 24 h under moderate shaking. Finally, the antibody−nanorod conjugates were washed twice in 0.1 M sodium phosphate buffer (pH 7.5) by centrifugation to remove unbound antibodies. After the final wash, the antibody−nanorod conjugates were redispersed in buffer or phenol free cell culture media.

For fluorescence imaging experiments, the antibodies with oxidized carbohydrate moieties were labeled with AlexaFlour dye (Invitrogen, A-20186) before attachment of the heterofunctional linker. The labeling was carried out using Invitrogen antibody labeling kit.

Amount of Antibodies per Nanorod. Gold nanorods were conjugated with fluorescently labeled antibodies in order to quantify the number of antibodies per nanorod. First, a calibration curve was plotted by measuring fluorescent emission peak intensity as a function of known concentrations of fluorescently labeled antibodies mixed with PEGylated nanorods at optical density of 0.1 cm^{-1}. The calibration measurements were carried out in the presence of nanorods to account for a decrease in fluorescence signal due to absorbance by gold nanorods. Then, suspensions of nanorod conjugates with fluorescently labeled antibodies were thoroughly washed to remove any residual free antibody molecules and were diluted to the optical density of 0.1 cm^{-1} to match the calibration measurements. The fluorescence emission of the conjugates was measured and the number of conjugated antibodies was determined using the calibration curve. To calculate the amount of antibodies per nanorods, we carefully analyzed the average size of the nanoparticles using transmittance electron microscopy (TEM) and gold concentration using inductively

dx.doi.org/10.1021/bc3004815 | Bioconjugate Chem. 2013, 24, 878−888

coupled plasma mass spectrometry on an Agilent ICP-MS system.

Specificity of Molecular Labeling. EGFR expressing human A431 cells and EGFR-negative human MDA-MB-435 cells were cultured in phenol-free DMEM (Invitrogen, 11039) and MEM (Invitrogen, 41061) culture media, respectively, supplemented with 10% fetal bovine serum (FBS) at 37 °C in a 5% CO2 environment. Antibody conjugated gold nanorods were incubated with either A431 cells or MDA-MB-435 cells for two hours at room temperature at a concentration of approximately 2×10^6 cells per milliliter of conjugated nanorods (at the same nanorod concentration as as-prepared nanorods). Unbound gold conjugates were separated from cells by centrifugation at $200 \times g$ for 3 min followed by washing cells with cell culture media. The labeled cells were characterized by UV−vis spectroscopy (BioTek Synergy HT) and optical microscopy. Bright-field transmittance and fluorescence (Cy5 filter cube, ex/em −649/670 nm) images were taken with Leica DM600 upright microscope, and the hyperspectral images were acquired using a PARISS spectral imager (Lightform Inc.). For all imaging, 20 × 0.5 NA objective and 100 W halogen light source were used. The hyperspectral system was calibrated using a standard low pressure Hg wavelength calibration lamp (Lightform, Inc.). The hyperspectral images obtained from cells were normalized by the lamp spectrum obtained from the part of the microscope slide that did not have cells. RGB images were taken using a 12-bit color mosaic CCD camera (SPOT Pursuit XS, Diagnostic Instruments).

Cell Viability Study. Biocompatibility of nanorods was characterized using MTS assay after incubation of A431, MDA-MB-435, and murine macrophage (J774A.1) cells with either 0.3 nM CTAB-NRs or PEG-NRs in phenol-free DMEM cell culture media supplemented with 10% FBS for 6 h at 37 °C. After removal of nanorods and washing once with PBS, the MTS reagent (mixture of MTS (3-(4,5-dimethylthiazol-2-yl)-5-(3-carboxymethoxyphenyl)-2-(4-sulfophenyl)-2*H*-tetrazolium) (Promega, G111B) and PMS (phenazine methosulfate) (Sigma, P9625) prepared in cell culture media) was added to the cells treated with nanorods and to untreated control cells. Absorbance at 490 nm wavelength is proportional to the number of metabolically active live cells in a sample.

Tissue Mimicking Phantom Preparation. Gelatin-based tissue mimicking phantoms with cell inclusions were fabricated for combined photoacoustic and ultrasound imaging. To simulate tissue background, 6% gelatin solution with 0.1 wt % of 15 μm silica particles was used to prepare base and top layers which encapsulated cell inclusions. Specifically, suspension of A431 cells only and A431 cells labeled with anti-EGFR gold nanorods were prepared at concentration of 4×10^7 cells/mL. Each cell suspension was mixed with the same volume of 12 wt % gelatin solution containing 0.2 wt % 15 μm silica particles at 37 °C. The mixture of cells and gelatin was placed on the base layer of 6 wt % gelatin with 0.1 wt % silica particles. Then, the top layer of gelatin/silica particles was added to complete the phantom.

Photoacoustic Imaging Setup. The ultrasound and photoacoustic imaging system consists of a microprocessor unit that utilizes a custom-built LabVIEW program to allow synchronization between the ultrasound pulser/receiver, data acquisition unit, pulsed laser, and 3D motion axis. Figure 3 depicts the imaging setup used in this study. The images were taken using 25 MHz single element focused transducer (f/# = 4, focal length = 25.4 mm), and the excitation light was

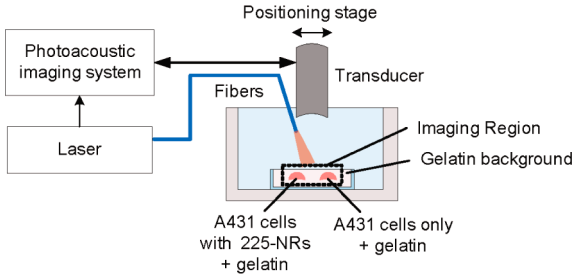

Figure 3. Schematic of the experimental setup used to obtain combined ultrasound and photoacoustic images.

delivered by a 1.5 mm diameter optical fiber. A tunable OPO laser with 7 ns pulse duration and 10 Hz pulse repetition rate was used to generate photoacoustic signal. The 2D ultrasound and photoacoustic images were obtained by mechanically scanning over the region of interest with 100 μm lateral step. To improve signal-to-noise ratio, 10 photoacoustic A-lines were collected and averaged.

X-ray Photoelectron Spectroscopy (XPS). XPS data was acquired using a Kratos AXIS Ultra DLD spectrometer equipped with a monochromatic Al X-ray source (Al α, 1.4866 keV). High resolution elemental analysis was performed on the O 1s, C 1s, N 1s, S 2p, and Au 4f regions with a 40 eV pass energy, utilizing 0.1 eV steps, and dwell time of 4 s per step. Charge compensation was used for the CTAB and PEG controls, in addition to CTAB and PEG-coated nanorods. All absolute energies were calibrated relative to gold and graphite. The peak positions and areas are calculated using a standard sum Gaussian−Lorentzian fit with a linear (O, C, N, S) or Shirley (Au) background correction.

RESULTS

The overall schematic of the conjugation process is shown in Figure 2. CTAB coated gold nanorods have high positive surface charge due to the presence of cationic surfactant (Table 1). After replacement of CTAB with mPEG-SH the surface

Table 1. Changes in Surface Charge of Gold Nanorods after Modifications with mPEG-Thiol Molecules and with Antibodies

Type of nanorods	Zeta potential, mV
CTAB-NRs	50.34 ± 0.8
PEG-NRs	8.33 ± 0.46
225-NRs	−16.26 ± 1.55
RG16-NRs	−24.34 ± 0.54

potential decreases from 50 mV for CTAB-coated nanorods to approximately 8 mV for mPEG-coated nanorods. These values correlate well with previously published ones[78] as we observed the same decrease in the zeta potential after modification of nanorods with mPEG-thiol molecules. TEM images of CTAB-coated and PEG-coated nanorods show no change in morphology of nanorods after removal of CTAB layer (Figure 4a).

To confirm that CTAB was replaced by PEG, high resolution X-ray photoelectron spectroscopy (XPS) was performed on CTAB-coated and PEG-coated nanorods. A similar analytical analyses was recently reported by Griesser et al.[81] The C 1s, O 1s, N 1s, S 2p, and Au 4f core level spectra from both nanorod samples and from pure CTAB and PEG were collected and

dx.doi.org/10.1021/bc3004815 | *Bioconjugate Chem.* 2013, 24, 878−888

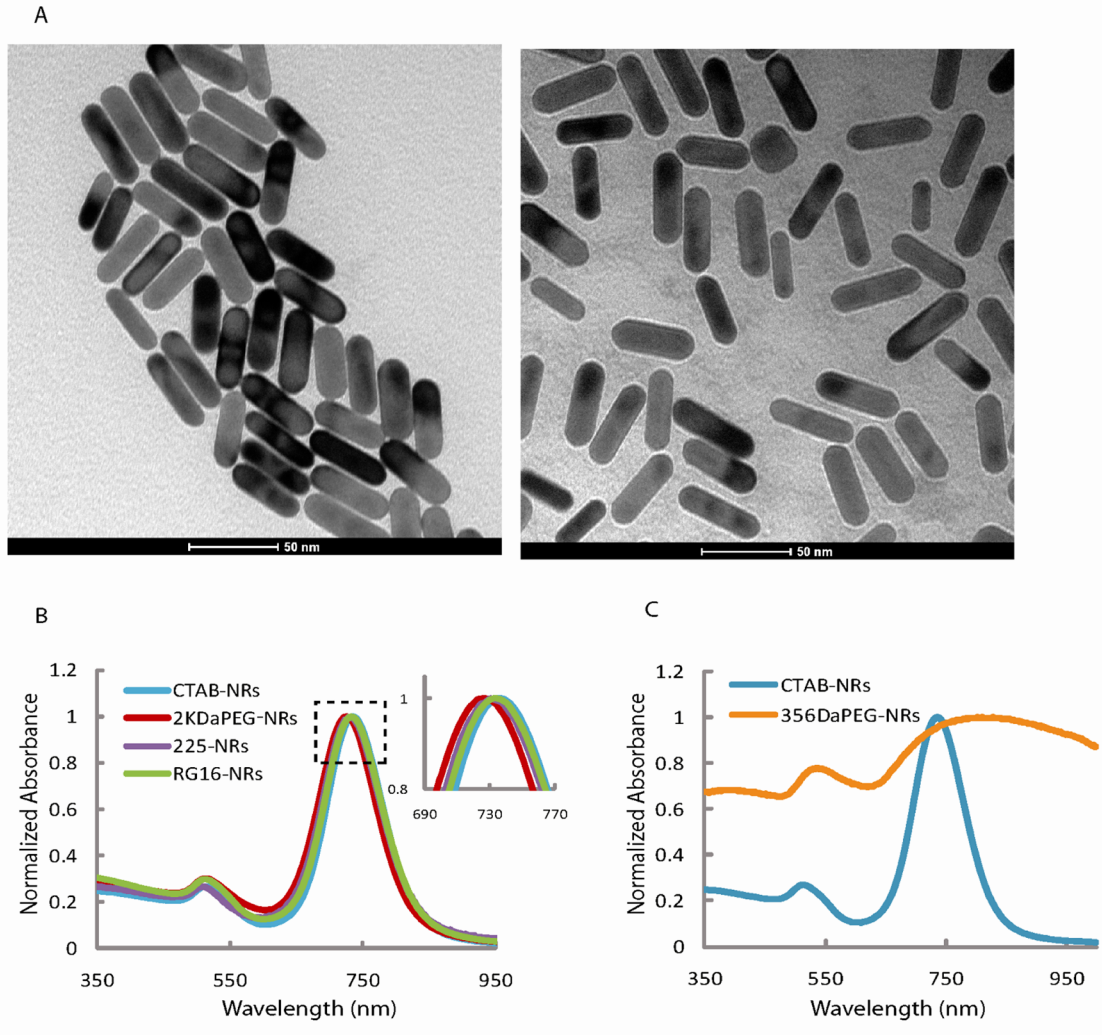

Figure 4. (a) Transmittance electron microscopy images of as prepared CTAB coated gold nanorods (left) and the nanorods after modification with mPEG-thiol molecules (right). (b) Extinction spectra of as prepared gold nanorods (blue) and the nanorods after modification with 2 kDa mPEG-thiol (red); clone c225 (purple), and RG16 (green) antibodies. (c) Comparison of extinction spectra of as prepared gold nanorods (blue) and nanorods after ligand exchange using small molecular weight, 356 Da MW, mPEG-thiol molecules (orange). Aggregation of nanorods is evident from profound spectral changes (orange spectrum).

analyzed. The spectra for CTAB-coated nanorods showed four core level regions: O 1s (1.5 rel. at.%), C 1s (92.5 rel. at.%), N 1s (4 rel. at.%), and Au (2 rel. at.%) (Figure S1). The C 1s spectrum consisted principally of $(-CH_2-CH_2-)_n$ functionality (285 eV), but displayed slight asymmetry. The very low signal from Au is most likely due photoelectron scattering in the dense CTAB bilayer. The spectra of PEG-coated nanorods revealed five core levels: O 1s (19 rel. at.%), C 1s (65 rel. at.%), N 1s (2 rel. at. %), S 2p (1 rel. at. %), and Au 4f (13 rel. at.%). The C 1s spectrum of PEG-coated nanorods differed greatly from that of CTAB-coated particles. The spectrum showed two peaks corresponding to two chemical states (Figure S1). The deconvolution of these two peaks revealed PEG functionality ($(-CH_2-CH_2-O_2-)_n$, 286.5 eV, 60 rel. at.% of C 1s) and CTAB functionality ($(-CH_2-CH_2-)_n$, 285 eV, 40 rel. at.%) (Figure S1). Additionally, an order of magnitude increase in O 1s signal at 532.8 eV, interpreted as a C−O functionality, clearly demonstrates the presence of $(-CH_2-CH_2-O-)_n$ repeat units of PEG molecules.[82] Furthermore, the increase in Au signal indicates that the Au 4f core level photoelectrons experience fewer scattering events. This is consistent with the exchange of the CTAB bilayer for a less-dense PEG layer.

The percentage of residual CTAB molecules after replacement with PEG was calculated using the XPS data and previously reported footprints of mPEG polymers[83] and CTAB molecules.[84] Because mPEG molecules can attach to surfaces at high (brush conformation) or low (mushroom conformation)[83] densities, the residual amount of CTAB on nanorod surface can vary from ca. 2.3% to 7.1% as compared to the initial CTAB surface coating for low and high PEG density, respectively (Supporting info for detailed calculations). The corresponding changes in zeta potential from ca. +50 mV for CTAB nanorods to ca. +8 mV for PEG nanorods suggest a high density confirmation of PEG molecules on the surface of nanorods (Table 1). Zeta potential measurements indicate approximately 16% of residual positive charge on the surface of PEG-coated nanorods as compared to CTAB nanorods while XPS measurements show 7.1% of residual CTAB surface coverage for a high density PEG conformation. This discrepancy might be due to an increased contribution to the positive zeta

dx.doi.org/10.1021/bc3004815 | *Bioconjugate Chem.* 2013, 24, 878−888

potential by the CTAB molecules adjacent to the gold surface in a CTAB bilayer that is disrupted by PEG molecules.

After completion of CTAB replacement with mPEG-SH, dithiol-linked antibodies were added to the PEGylated nanorods. The linker was attached to the Fc antibody moiety to achieve directional conjugation on the gold surface. Two types of antibodies were used in this study: EGFR specific clone 225 and nonspecific antirabbit IgG clone RG-16. Conjugation of antibodies results in decrease in zeta potential to −16 and −24 mV in the case of clone 225 and clone RG-16, respectively (Table 1). The observed negative zeta potential changes correlate well with literature[85] and provide indirect evidence of antibody conjugation. We achieved 6.5 ± 1.8 antibodies conjugated per nanorod based on fluorescence emission spectra of nanorod−conjugates prepared with fluorescently labeled antibodies.

Extinction spectra show ca. 8 nm blue shift of the longitudinal peak of the PEGylated nanorods as compared to CTAB-nanorods with no peak broadening (Figure 4b). Attachment of antibodies results in approximately 6 nm red shift of the longitudinal peak relative to the PEGylated nanoparticles for both 225 and RG-16 modified nanorods. The observed spectral shifts can be attributed to changes in the refractive index of the local environment surrounding the nanorods. This effect has been well documented in the literature.[86,87] The spectral characterization also provides an important and simple way to monitor possible aggregation of plasmonic nanoparticles during a conjugation procedure. This process can be easily monitored using characteristic spectral changes associated with nanorod aggregation that include three major features: significant broadening and strong red shift of the longitudinal peak as well as increase in transverse to longitudinal (T-to-L) peak ratio (Figure 4c). The molecular targeted nanorods synthesized using conjugation strategy proposed here show mean value of T-to-L peak ratio increase of less than 9% (Table 2). In addition, the full-width at half-maximum of the longitudinal peak does not increase with the PEGylation or antibody conjugation as evident from Figure 4b and Table 2. These spectroscopic data confirm that nanorods do not aggregate during conjugation with antibodies.

Table 2. Spectral Characteristics of Gold Nanorods and Gold Nanorod Conjugates

	FW at HM, nm	% increase in transverse to longitudinal peak ratio
CTAB-Nanorods	109.7 ± 7.4	
mPEG(2K Da)-Nanorods	100.5 ± 7.5	8.1 ± 2.1
225Ab-Nanorods	107 ± 4.6	8.9 ± 2.8
mPEG(356 Da)-Nanorods	337.3 ± 66.1	277.4 ± 44.0

It is important to note that the molecular weight of mPEG-SH molecules used to replace CTAB layer during the first conjugation step is very important. In this study, 2 KDa mPEG-SH was used to produce stable molecular targeted nanorods. The use of lower molecular weight 356 Da mPEG-SH led to nanoparticle aggregation as evident from significant broadening and a more than 100 nm red shift of the longitudinal peak and an increase of more than 250% in the T-to-L peak ratio (Figure 4c and Table 2). The use of higher molecular weight 5 kDa mPEG-SH resulted in stable nanorod suspensions. However, attempts to conjugate antibodies to these nanorods failed as they did not label EGFR expressing cells. This can be attributed to a steric hindrance effect that did not allow antibodies to replace high molecular weight PEG molecules from nanorod surface.

CTAB coated gold nanorods are known to have cytotoxic effects.[88,89] Therefore, we characterized cellular toxicity of nanorods after replacement of CTAB with mPEG-SH molecules. The cell viability study was performed using two different cancer cell lines (EGFR expressing A431 and EGFR negative MDA-MB-435) and a macrophage cell line (J774A.1). As expected, the CTAB-coated nanorods were highly toxic in all cell lines (Figure 5). Replacement of CTAB with mPEG-SH resulted in biocompatible nanorods which did not exhibit cytotoxic effects in any of the cell lines studied (Figure 5).

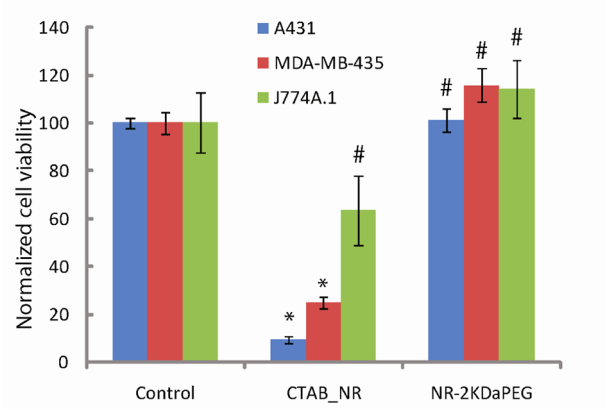

Figure 5. Cytotoxicity of as prepared CTAB coated and 2 kDa mPEG-thiol coated nanorods in different cell lines. The *y*-axis shows normalized cell viability. The viability of control samples is normalized to 100. Values statistically different ($p < 0.05$) from controls are labeled by *; values that do not show statistically significant difference from controls ($p > 0.05$) are labeled by #.

Molecular specificity of the antibody conjugated nanorods was evaluated in two cell lines: EGFR-positive A431 and EGFR-negative MDA-MB-435 cells. Molecular targeted nanorods were conjugated with anti-EGFR clone 225 antibodies and nanorods conjugated with nonspecific clone RG-16 antibodies were used as control. Figure 6 shows dark-field and transmittance hyperspectral images of labeled cells and controls. Only EGFR-positive A431 cells labeled with antiEGFR nanorods show distinct spectral signatures in the 500−800 nm range which corresponds to gold nanorods. There is no detectable difference between unlabeled cells and both the EGFR-positive A431 cells labeled with nontargeted RG-16 conjugated nanorods and the EGFR-negative MDA-MD-435 cells labeled with anti-EGFR nanorods. Conjugates of nanorods with fluorescently labeled anti-EGFR antibodies were also used to label both the EGFR positive and the EGFR negative cell lines; a strong fluorescent signal was observed only from labeled EGFR-positive A431 cells (Figure S2). These results demonstrate molecular specificity of gold nanorods conjugated with anti-EGFR antibodies.

Dark-field reflected image of A431 cells labeled with molecular targeted nanorods appears greenish yellow to orange as compared to unlabeled cells due to light reflection by the nanorods (Figure 6, second row). Analyses of bright-field transmittance and hyperspectral transmittance images revealed strong absorbance above 700 nm throughout labeled cells. The

dx.doi.org/10.1021/bc3004815 | *Bioconjugate Chem.* 2013, 24, 878−888

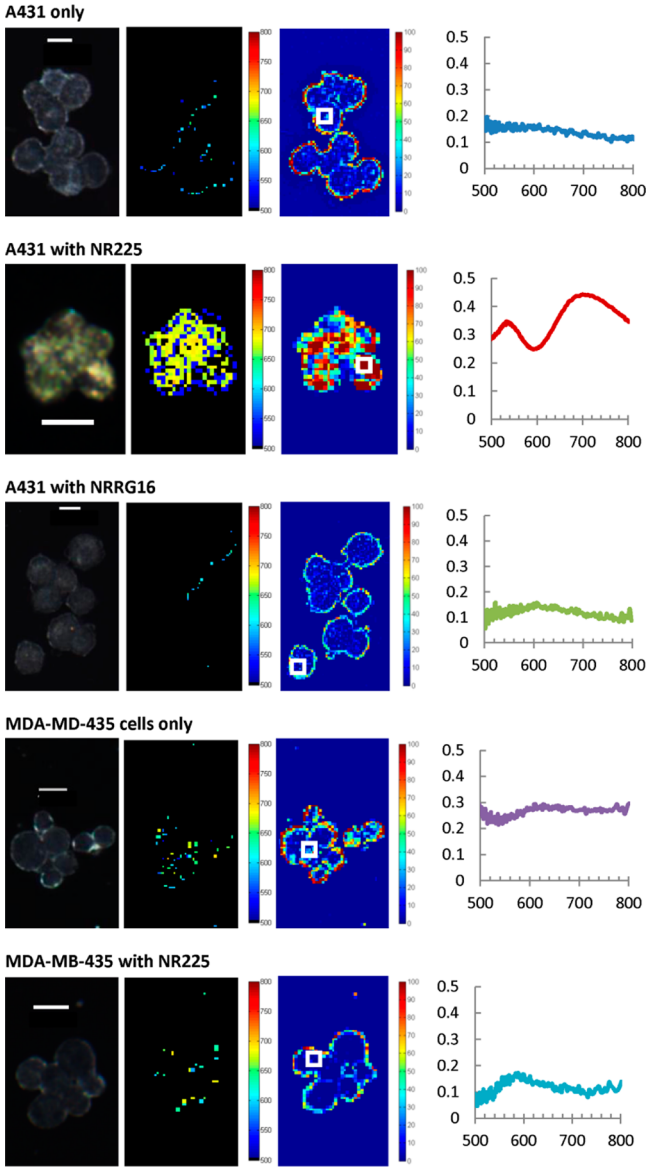

Figure 6. Optical characterization of molecular specificity of antibody conjugated gold nanorods in cell cultures. Columns from left to right: reflected dark-field images; transmittance hyperspectral image with color coded peak wavelength in the 500−800 nm spectral region; transmittance hyperspectral image with color coded integrated absorbance in the 500−800 nm region; absorbance spectra integrated over the regions highlighted by white squares in the previous column.

absorbance spectra of the nanorod labeled cells is broadened with the full-width at half-maximum of 150 ± 7.6 nm as compared to 107 ± 4.6 nm in the case of nanorods in suspension. In addition, the T-to-L peak ratio increases by 52 ± 21.31% relative to isolated nanorods. These optical changes can be attributed to EGF receptor mediated aggregation of nanorods. The same effect has been observed and thoroughly characterized by our group in the case of EGFR targeted spherical plasmonic nanoparticles.[1,29,90]

It is of interest to note that there is a perception of an increased absorption at cellular boundaries in hyperspectral transmittance images (Figure 6). This effect is due to light diffraction at the interface between cells and the surrounding medium. However, these boundary regions in control samples do not exhibit spectral signatures of gold nanorods.

EGFR-positive A431 cells labeled with anti-EGFR nanorods exhibit strong contrast in photoacoustic imaging (Figure 7).

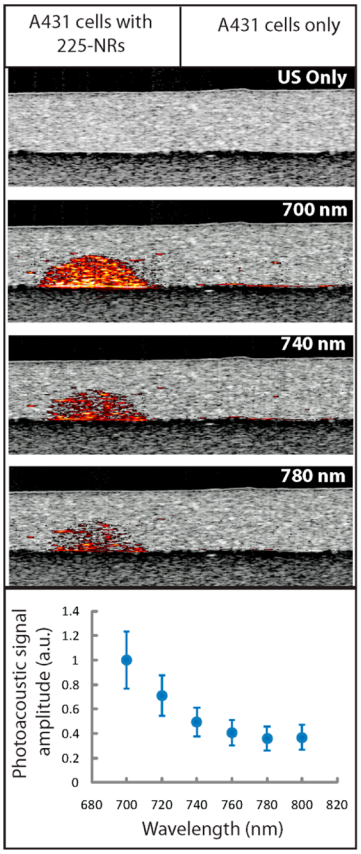

Figure 7. Combined ultrasound (US) and photoacoustic (PA) images of tissue mimicking cell phantoms. The phantom on the left consists of A431 cells labeled with anti-EGFR gold nanorods and the phantom on the right has unlabeled A431 cells. The plot at the bottom shows PA signal intensity integrated over the phantom area as a function of excitation wavelength.

Multi wavelength photoacoustic imaging was used to obtain spectral characteristics of the labeled cells. The intensity of the photoacoustic signal decreases as a function of wavelength in the 700−800 nm wavelength region; this behavior is in good agreement with extinction spectra of the labeled cells (compare Figure 6, second row, and Figure 7). Note that gold nanorods with 700 nm extinction maximum were used in these imaging experiments. As expected, the unlabeled A431 cells did not produce any photoacoustic signal.

DISCUSSION

Directional conjugation involves achievement of a high level of control over an orientation of a biomolecule on nanoparticle surface. Orientation is particularly important in the conjugation of antibodies to the particle surface as many potential orientations of the antibody lead to a loss of antibody binding function, but in general orientation is also quite important for other proteins and molecules. Directional conjugation can be accomplished for molecules that have uniquely accessible functional groups. In the case of antibodies, one such functional group is the carbohydrate moiety located on the heavy chain of most antibodies. It was previously demonstrated that periodate-mediated oxidation of the carbohydrate group located on the

dx.doi.org/10.1021/bc3004815 | Bioconjugate Chem. 2013, 24, 878−888

Fc- region of an antibody to an aldehyde can be used for oriented conjugation of monoclonal antibodies to an immunopurification matrix containing hydrazide functional groups; the resulting matrix yielded the antigen-binding activity close to the theoretical value of 2 mol of bound antigens per 1 mol of a conjugated antibody. [80] In this study a heterofunctional linker with hydrazide and dithiol groups on opposing sites of the molecule was used to achieve directional conjugation of antibodies to gold nanorods. The hydrazide moiety interacts with the aldehyde on the antibody and the dithiol enables conjugation directly to the gold surface.[79] It is important to note that linkers with two adjacent sulfhydryl groups such as thioctic acid provide greater stability as compared to a single sulfhydryl group.[85] It has been shown that molecules conjugated using single sulfhydryl-containing linkers can be replaced in biological environment by an excess of naturally present sulfhydryl-containing biomolecules such as glutathione.[51]

Previously published methods of synthesis of gold nanorod bioconjugates have several downsides including lower *in vivo* stability of bioconjugates produced by electrostatic interactions, cytotoxicity due to presence of CTAB in final nanorods conjugates, and lack of control over antibody orientation during conjugation. In addition, most literature reports provide insufficient characterization of prepared conjugates that makes assessment of nanorod conjugates quality difficult.

Important information pertaining to the aggregation state and stability of nanorod conjugates can be obtained from nanorod extinction spectra before and after conjugation. For example, percentage change in the transverse to longitudinal (T-to-L) peak ratio is one spectral parameter that can be used in evaluation and comparison of nanorod conjugation approaches; other parameters include spectral shift and full-width at half-maximum of the longitudinal peak. In addition, zeta potential measurements can provide insight into changes of surface composition during conjugation reaction steps. Unfortunately, most previously published reports do not include analyses of nanorod extinction spectra before and after conjugation with antibodies. The importance of this characterization can be illustrated using an example from a recently published conjugation approach where bioconjugated nanorods were prepared by, first, replacing the CTAB layer with 11-mercapto undecanoic acid (MUDA) and then attaching antibody fragments through primary amino groups to the carboxylic acid groups of MUDA using EDC chemistry.[58] The nanorods with geometrical aspect ratios 2.3 and 3.5 showed approximately 64.7% and 23.5% increase in the T-to-L peak ratio after CTAB replacement with MUDA, respectively, as can be calculated from the published spectra. These changes can indicate potential aggregation of nanorods during the conjugation procedure. In contrast, molecular specific nanorods synthesized using the technique reported here undergo increase in the mean value of T-to-L peak ratio of less than 9% (Table 2). In addition, there are no changes in the full-width at half-maximum of the longitudinal peak during conjugation procedure or after antibody conjugation.

CONCLUSIONS

In this study, we have developed a robust conjugation technique for reproducible synthesis of molecular specific gold nanorods and have fully characterized conjugates using zeta potential, UV−vis spectra, electron microscopy, and hyperspectral optical imaging. Furthermore, the nanorod bioconjugates were prepared by attaching the Fc portion of antibodies to the nanorod surface that has two important advantages: first, directional attachment of antibodies through nonbinding Fc moieties provides maximum possible binding efficiency of the conjugates; second, since the Fc moieties in the conjugates are oriented toward nanorod surface, they are not available for interaction with Fc receptors that are present in some human cells including macrophages, consequently, this could significantly improve stealth properties of the nanoparticles providing longer residence time and diminishing potential immunogenicity in *in vivo* applications. We demonstrated that molecular specific gold nanorods synthetized here can be used to image cancer cells using optical and photoacoustic imaging modalities. Additionally, we observed characteristic changes in optical spectra of molecular targeted nanorods after their uptake by cancer cells; the observed spectral signatures can be explored for sensitive detection of interactions between molecular specific nanoparticles and cells.

ASSOCIATED CONTENT

Supporting Information

XPS spectra; Calculation of residual CTAB on PEG-coated nanorods; Fluorescence images of cells labeled with nanorods. This material is available free of charge via the Internet at http://pubs.acs.org.

AUTHOR INFORMATION

Corresponding Author

*E-mail: kostia@mail.utexas.edu.

Notes

The authors declare no competing financial interest.

ACKNOWLEDGMENTS

We acknowledge National Institute of Health grants EB008101, HL096981, and CA149740 for partial financial support of this research. The Kratos XPS was funded by the NSF under grant CHE-0618242.

REFERENCES

(1) Sokolov, K., Follen, M., Aaron, J., Pavlova, I., Malpica, A., Lotan, R., and Richards-Kortum, R. (2003) Real-time vital optical imaging of precancer using anti-epidermal growth factor receptor antibodies conjugated to gold nanoparticles. *Cancer Res. 63*, 1999−2004.

(2) Sokolov, K., Aaron, J., Hsu, B., Nida, D., Gillenwater, A., Follen, M., MacAulay, C., Adler-Storthz, K., Korgel, B., Descour, M., Pasqualini, R., Arap, W., Lam, W., and Richards-Kortum, R. (2003) Optical systems for in vivo molecular imaging of cancer. *Technology in Cancer Research & Treatment 2*, 491−504.

(3) Hirsch, L. R., Stafford, R. J., Bankson, J. A., Sershen, S. R., Rivera, B., Price, R. E., Hazle, J. D., Halas, N. J., and West, J. L. (2003) Nanoshell-mediated near-infrared thermal therapy of tumors under magnetic resonance guidance. *Proc. Natl. Acad. Sci. U.S.A. 100*, 13549−13554.

(4) Parak, W. J., Gerion, D., Pellegrino, T., Zanchet, D., Micheel, C., Williams, S. C., Boudreau, R., Le Gros, M. A., Larabell, C. A., and Alivisatos, A. P. (2003) Biological applications of colloidal nanocrystals. *Nanotechnology 14*, R15−R27.

(5) Loo, C., Lin, A., Hirsch, L., Lee, M.-H., Barton, J., Halas, N., West, J., and Drezek, R. (2004) Nanoshell-enabled photonics-based imaging and therapy of cancer. *Technology in Cancer Research & Treatment 3*, 33−40.

(6) Alivisatos, P. (2004) The use of nanocrystals in biological detection. *Nat. Biotechnol. 22*, 47−52.

(7) El-Sayed, I. H., Huang, X., and El-Sayed, M. A. (2005) Surface plasmon resonance scattering and absorption of anti-EGFR antibody

conjugated gold nanoparticles in cancer diagnostics: Applications in oral cancer. *Nano Lett. 5*, 829−834.
(8) Loo, C., Lowery, A., Halas, N., West, J., and Drezek, R. (2005) Immunotargeted Nanoshells for Integrated Cancer Imaging and Therapy. *Nano Lett. 5*, 709−711.
(9) Aslan, K., Lakowicz, J. R., and Geddes, C. D. (2005) Plasmon light scattering in biology and medicine: new sensing approaches, visions and perspectives. *Curr. Opin. Chem. Biol. 9*, 538−544.
(10) Huang, X., El-Sayed, I. H., Qian, W., and El-Sayed, M. A. (2006) Cancer Cell Imaging and Photothermal Therapy in the Near-Infrared Region by Using Gold Nanorods. *J. Am. Chem. Soc. 128*, 2115−2120.
(11) Liu, G. L., Yin, Y., Kunchakarra, S., Mukherjee, B., Gerion, D., Jett, S. D., Bear, D. G., Gray, J. W., Alivisatos, A. P., Lee, L. P., and Chen, F. F. (2006) A nanoplasmonic molecular ruler for measuring nuclease activity and DNA footprinting. *Nat. Nano 1*, 47−52.
(12) Larson, T. A., Bankson, J., Aaron, J., and Sokolov, K. (2007) Hybrid plasmonic magnetic nanoparticles as molecular specific agents for MRI/optical imaging and photothermal therapy of cancer cells. *Nanotechnology 18*, 325101.
(13) Mallidi, S., Larson, T., Aaron, J., Sokolov, K., and Emelianov, S. (2007) Molecular specific optoacoustic imaging with plasmonic nanoparticles. *Opt. Express 15*, 6583−6588.
(14) Yang, X., Skrabalak, S. E., Li, Z. Y., Xia, Y., and Wang, L. V. (2007) Photoacoustic tomography of a rat cerebral cortex in vivo with Au nanocages as an optical contrast agent. *Nano Lett. 7*, 3798−3802.
(15) Chen, J., Wang, D., Xi, J., Au, L., Siekkinen, A., Warsen, A., Li, Z.-Y., Zhang, H., Xia, Y., and Li, X. (2007) Immuno gold nanocages with tailored optical properties for targeted photothermal destruction of cancer cells. *Nano Lett. 7*, 1318−1322.
(16) Anker, J. N., Hall, W. P., Lyandres, O., Shah, N. C., Zhao, J., and Van Duyne, R. P. (2008) Biosensing with plasmonic nanosensors. *Nat. Mater. 7*, 442−453.
(17) Skala, M. C., Crow, M. J., Wax, A., and Izatt, J. A. (2008) Photothermal optical coherence tomography of epidermal growth factor receptor in live cells using immunotargeted gold nanospheres. *Nano Lett. 8*, 3461−3467.
(18) Curry, A., Crow, M. J., and Wax, A. (2008) Molecular imaging of epidermal growth factor receptor in live cells with refractive index sensitivity using dark-field microspectroscopy and immunotargeted nanoparticles. *J. Biomed. Opt. 13*, 014022.
(19) Jain, P. K., Huang, X., El-Sayed, I. H., and El-Sayed, M. A. (2008) Noble metals on the nanoscale: optical and photothermal properties and some applications in imaging, sensing, biology, and medicine. *Acc. Chem. Res. 41*, 1578−1586.
(20) Lee, S. E., and Lee, L. P. (2010) Biomolecular plasmonics for quantitative biology and nanomedicine. *Curr. Opin. Biotechnol. 21*, 489−497.
(21) Chanda, N., Kattumuri, V., Shukla, R., Zambre, A., Katti, K., Upendran, A., Kulkarni, R. R., Kan, P., Fent, G. M., Casteel, S. W., Smith, C. J., Boote, E., Robertson, J. D., Cutler, C., Lever, J. R., Katti, K. V., and Kannan, R. (2010) Bombesin functionalized gold nanoparticles show in vitro and in vivo cancer receptor specificity. *Proc. Natl. Acad. Sci. U. S. A. 107*, 8760−8765.
(22) Crow, M. J., Marinakos, S. M., Cook, J. M., Chilkoti, A., and Wax, A. (2011) Plasmonic flow cytometry by immunolabeled nanorods. *Cytometry Part A: Journal of the International Society for Advancement of Cytometry 79*, 57−65.
(23) Chanda, N., Shukla, R., Zambre, A., Mekapothula, S., Kulkarni, R., Katti, K., Bhattacharyya, K., Fent, G., Casteel, S., Boote, E., Viator, J., Upendran, A., Kannan, R., and Katti, K. (2011) An effective strategy for the synthesis of biocompatible gold nanoparticles using cinnamon phytochemicals for phantom CT imaging and photoacoustic detection of cancerous cells. *Pharm. Res. 28*, 279−291.
(24) Prigodich, A. E., Alhasan, A. H., and Mirkin, C. A. (2011) Selective enhancement of nucleases by polyvalent DNA-functionalized gold nanoparticles. *J. Am. Chem. Soc. 133*, 2120−2123.
(25) Dreaden, E. C., Mackey, M. A., Huang, X., Kang, B., and El-Sayed, M. A. (2011) Beating cancer in multiple ways using nanogold. *Chem. Soc. Rev. 40*, 3391−3404.
(26) Bharill, S., Chen, C., Stevens, B., Kaur, J., Smilansky, Z., Mandecki, W., Gryczynski, I., Gryczynski, Z., Cooperman, B. S., and Goldman, Y. E. (2010) Enhancement of single-molecule fluorescence signals by colloidal silver nanoparticles in studies of protein translation. *ACS Nano 5*, 399−407.
(27) Lee, K. M., Neogi, A., Basu Neogi, P., Kim, M., Kim, B., Luchowski, R., Gryczynski, Z., Calander, N., and Choi, T. Y. (2011) Silver nanostructure sensing platform for maximum-contrast fluorescence cell imaging. *J. Biomed. Opt. 16*, 056008.
(28) Matteini, P., Ratto, F., Rossi, F., and Pini, R. (2012) Emerging concepts of laser-activated nanoparticles for tissue bonding. *J. Biomed. Opt. 17*, 010701.
(29) Aaron, J., Nitin, N., Travis, K., Kumar, S., Collier, T., Park, S. Y., Jose-Yacaman, M., Coghlan, L., Follen, M., Richards-Kortum, R., and Sokolov, K. (2007) Imaging of epidermal growth factor receptor in early carcinogenesis using plasmon resonance coupling of metal nanoparticles. *J. Biomed. Opt. 12*, 034007.
(30) Liu, G. L., Yin, Y., Kunchakarra, S., Mukherjee, B., Gerion, D., Jett, S. D., Bear, D. G., Gray, J. W., Alivisatos, A. P., Lee, L. P., and Chen, F. F. (2006) A nanoplasmonic molecular ruler for measuring nuclease activity and DNA footprinting. *Nat. Nanotechnol. 1*, 47−52.
(31) Wax, A., and Sokolov, K. (2009) Molecular imaging and darkfield microspectroscopy of live cells using gold plasmonic nanoparticles. *Laser & Photonics Reviews 3*, 146−158.
(32) Mercatelli, R., Romano, G., Ratto, F., Matteini, P., Centi, S., Cialdai, F., Monici, M., Pini, R., and Fusi, F. (2011) Quantitative measurement of scattering and extinction spectra of nanoparticles by darkfield microscopy. *Appl. Phys. Lett. 99*.
(33) Wang, H., Huff, T. B., Zweifel, D. A., He, W., Low, P. S., Wei, A., and Cheng, J.-X. (2005) In vitro and in vivo two-photon luminescence imaging of single gold nanorods. *Proc. Natl. Acad. Sci. U.S.A. 102*, 15752−15756.
(34) Durr, N. J., Larson, T., Smith, D. K., Korgel, B. A., Sokolov, K., and Ben-Yakar, A. (2007) Two-photon luminescence imaging of cancer cells using molecularly targeted gold nanorods. *Nano Lett. 7*, 941−945.
(35) Park, J., Estrada, A., Sharp, K., Sang, K., Schwartz, J. A., Smith, D. K., Coleman, C., Payne, J. D., Korgel, B. A., Dunn, A. K., and Tunnell, J. W. (2008) Two-photon-induced photoluminescence imaging of tumors using near-infrared excited gold nanoshells. *Opt. Express 16*, 1590−1599.
(36) Mallidi, S., Larson, T., Tam, J., Joshi, P. P., Karpiouk, A., Sokolov, K., and Emelianov, S. (2009) Multiwavelength photoacoustic imaging and plasmon resonance coupling of gold nanoparticles for selective detection of cancer. *Nano Lett. 9*, 2825−2831.
(37) Wang, B., Yantsen, E., Larson, T., Karpiouk, A. B., Sethuraman, S., Su, J. L., Sokolov, K., and Emelianov, S. Y. (2009) Plasmonic intravascular photoacoustic imaging for detection of macrophages in atherosclerotic plaques. *Nano Lett. 9*, 2212−2217.
(38) Oraevsky, A. A. (2009) Gold and silver nanoparticles as contrast agents for optoacoustic tomography. *Opt. Sci. Eng. 144*, 373−386.
(39) Ntziachristos, V., and Razansky, D. (2010) Molecular imaging by means of multispectral optoacoustic tomography (MSOT). *Chem. Rev. (Washington, DC, U. S.) 110*, 2783−2794.
(40) Ntziachristos, V. (2010) Going deeper than microscopy: the optical imaging frontier in biology. *Nat. Methods 7*, 603−614.
(41) Kim, C., Song, H. M., Cai, X., Yao, J., Wei, A., and Wang, L. V. (2011) In vivo photoacoustic mapping of lymphatic systems with plasmon-resonant nanostars. *J Mater Chem 21*, 2841−2844.
(42) Wang, L. V., and Hu, S. (2012) Photoacoustic tomography: in vivo imaging from organelles to organs. *Science 335*, 1458−1462.
(43) Liopo, A. V., Conjusteau, A., and Oraevsky, A. A. (2012) *Proc. SPIE*, 822344.
(44) Stern, J. M., Stanfield, J., Kabbani, W., Hsieh, J.-T., and Cadeddu, J. A. (2008) Selective prostate cancer thermal ablation with laser activated gold nanoshells. *J. Urol. 179*, 748−753.
(45) Baek, S. K., Makkouk, A. R., Krasieva, T., Sun, C. H., Madsen, S. J., and Hirschberg, H. (2011) Photothermal treatment of glioma; an in

vitro study of macrophage-mediated delivery of gold nanoshells. *J. Neurooncol. 104*, 439−448.
(46) Xia, Y., Li, W., Cobley, C. M., Chen, J., Xia, X., Zhang, Q., Yang, M., Cho, E. C., and Brown, P. K. (2011) Gold nanocages: from synthesis to theranostic applications. *Acc. Chem. Res. 44*, 914−924.
(47) Li, W., Cai, X., Kim, C., Sun, G., Zhang, Y., Deng, R., Yang, M., Chen, J., Achilefu, S., Wang, L. V., and Xia, Y. (2011) Gold nanocages covered with thermally-responsive polymers for controlled release by high-intensity focused ultrasound. *Nanoscale 3*, 1724−1730.
(48) Zharov, V. P., Galitovskaya, E. N., Johnson, C., and Kelly, T. (2005) Synergistic enhancement of selective nanophotothermolysis with gold nanoclusters: Potential for cancer therapy. *Lasers Surg. Med, 37*, 219−226.
(49) Cheong, W. F., Prahl, S. A., and Welch, A. J. (1990) A review of the optical properties of biological tissues. *IEEE Journal of Selected Topics in Quantum Electronics 26*, 2166−2185.
(50) Sowa, M., Leonardi, L., Matas, A., Schattka, B., Hewko, M., Payette, J., and Mantsch, H. (2000) Near infrared spectroscopy: in-vivo tissue analysis, in *Encyclopedia of Analytical Chemistry* (Meyers, R., Ed.) pp 251−281, John Wiley & Sons Ltd.
(51) Oishi, M., Nakaogami, J., Ishii, T., and Nagasaki, Y. (2006) Smart PEGylated gold nanoparticles for the cytoplasmic delivery of siRNA to induce enhanced gene silencing. *Chem. Lett. 35*, 1046−1047.
(52) Lee, S. E., Liu, G. L., Kim, F., and Lee, L. P. (2009) Remote optical switch for localized andselective control of gene interference. *Nano Lett. 9*, 562−570.
(53) Lu, W., Zhang, G., Zhang, R., Flores, L. G., Huang, Q., Gelovani, J. G., and Li, C. (2010) Tumor site−-specific silencing of NF-κB p65 by targeted hollow gold nanosphere-mediated photothermal transfection. *Cancer Res. 70*, 3177−3188.
(54) Huang, X., Neretina, S., and El-Sayed, M. A. (2009) Gold nanorods: from synthesis and properties to biological and biomedical applications. *Adv. Mater. (Weinheim, Ger.) 21*, 4880−4910.
(55) Nusz, G. J., Marinakos, S. M., Curry, A. C., Dahlin, A., Hook, F., Wax, A., and Chilkoti, A. (2008) Label-free plasmonic detection of biomolecular binding by a single gold nanorod. *Anal. Chem. 80*, 984−989.
(56) Tong, L., Wei, Q., Wei, A., and Cheng, J.-X. (2009) Gold nanorods as contrast agents for biological imaging: optical properties, surface conjugation and photothermal effects†. *Photochem. Photobiol. 85*, 21−32.
(57) Jain, P. K., Lee, K. S., El-Sayed, I. H., and El-Sayed, M. A. (2006) Calculated absorption and scattering properties of gold nanoparticles of different size, shape, and composition: applications in biological imaging and biomedicine. *J. Phys. Chem. B 110*, 7238−7248.
(58) Yu, C., and Irudayaraj, J. (2007) Multiplex biosensor using gold nanorods. *Anal. Chem. 79*, 572−579.
(59) Bayer, C. L., Chen, Y.-S., Kim, S., Mallidi, S., Sokolov, K., and Emelianov, S. (2011) Multiplex photoacoustic molecular imaging using targeted silica-coated gold nanorods. *Biomed. Opt. Express 2*, 1828−1835.
(60) Agarwal, A., Huang, S. W., O'Donnell, M., Day, K. C., Day, M., Kotov, N., and Ashkenazi, S. (2007) Targeted gold nanorod contrast agent for prostate cancer detection by photoacoustic imaging. *J. Appl. Phys. 102*, 064701−1.
(61) Cui, H., and Yang, X. (2010) In vivo imaging and treatment of solid tumor using integrated photoacoustic imaging and high intensity focused ultrasound system. *Medical Physics 37*, 4777−4781.
(62) Mallidi, S., Luke, G. P., and Emelianov, S. (2011) Photoacoustic imaging in cancer detection, diagnosis, and treatment guidance. *Trends Biotechnol. 29*, 213−221.
(63) Shah, J., Park, S., Aglyamov, S., Larson, T., Ma, L., Sokolov, K., Johnston, K., Milner, T. E., and Emelianov, S. Y. (2008) Photoacoustic imaging and temperature measurement for photothermal cancer therapy. *J. Biomed. Opt. 13*, 034024.
(64) Dickerson, E. B., Dreaden, E. C., Huang, X., El-Sayed, I. H., Chu, H., Pushpanketh, S., McDonald, J. F., and El-Sayed, M. A. (2008) Gold nanorod assisted near-infrared plasmonic photothermal therapy (PPTT) of squamous cell carcinoma in mice. *Cancer Lett. 269*, 57−66.
(65) Huang, X., El-Sayed, I. H., Qian, W., and El-Sayed, M. A. (2007) Cancer cells assemble and align gold nanorods conjugated to antibodies to produce highly enhanced, sharp, and polarized surface raman spectra: a potential cancer diagnostic marker. *Nano Lett. 7*, 1591−1597.
(66) Wang, G., Sun, W., Luo, Y., and Fang, N. (2010) Resolving rotational motions of nano-objects in engineered environments and live cells with gold nanorods and differential interference contrast microscopy. *J. Am. Chem. Soc. 132*, 16417−16422.
(67) Hauck, T. S., Ghazani, A. A., and Chan, W. C. W. (2008) Assessing the effect of surface chemistry on gold nanorod uptake, toxicity, and gene expression in mammalian cells. *Small 4*, 153−159.
(68) Murphy, C. J., Gole, A. M., Stone, J. W., Sisco, P. N., Alkilany, A. M., Goldsmith, E. C., and Baxter, S. C. (2008) Gold nanoparticles in biology: beyond toxicity to cellular imaging. *Acc. Chem. Res. 41*, 1721−1730.
(69) Lévy, R., Shaheen, U., Cesbron, Y., and Sée, V. (2010) Gold nanoparticles delivery in mammalian live cells: a critical review. *Nano Rev. 1*.
(70) Wei, A., Wei, Q., and Leonov, A. P. (2011) Gold Nanorods as Theranostic Agents, in *Nanoplatform-Based Molecular Imaging*, pp 659−681, John Wiley & Sons, Inc.
(71) Nikoobakht, B., and El-Sayed, M. A. (2003) Preparation and growth mechanism of gold nanorods (NRs) using seed-mediated growth method. *Chem. Mater. 15*, 1957−1962.
(72) Grabinski, C., Schaeublin, N., Wijaya, A., D'Couto, H., Baxamusa, S. H., Hamad-Schifferli, K., and Hussain, S. M. (2011) Effect of gold nanorod surface chemistry on cellular response. *ACS Nano 5*, 2870−2879.
(73) Perumal, S., Hofmann, A., Scholz, N., Rühl, E., and Graf, C. (2011) Kinetics study of the binding of multivalent ligands on size-selected gold nanoparticles. *Langmuir 27*, 4456−4464.
(74) Yu, C., Varghese, L., and Irudayaraj, J. (2007) Surface Modification of Cetyltrimethylammonium Bromide-Capped Gold Nanorods to make molecular probes. *Langmuir 23*, 9114−9119.
(75) Wei, C.-W., Liao, C.-K., Chen, Y.-Y., Wang, C.-R. C., Ding, A.-A., Shiehd, D.-B., and Li, P.-C. (2008) Photons Plus Ultrasound: Imaging and Sensing , In *2008: The Ninth Conference on Biomedical Thermoacoustics, Optoacoustics, and Acousto-optics*, pp 68560J−11, SPIE, San Jose, CA, USA.
(76) Liao, H., and Hafner, J. H. (2005) Gold Nanorod Bioconjugates. *Chem. Mater. 17*, 4636−4641.
(77) Eghtedari, M., Liopo, A. V., Copland, J. A., Oraevsky, A. A., and Motamedi, M. (2009) Engineering of hetero-functional gold nanorods for the in vivo molecular targeting of breast cancer cells. *Nano Lett 9*, 287−91.
(78) Niidome, T., Yamagata, M., Okamoto, Y., Akiyama, Y., Takahashi, H., Kawano, T., Katayama, Y., and Niidome, Y. (2006) PEG-modified gold nanorods with a stealth character for in vivo applications. *J. Controlled Release 114*, 343−347.
(79) Kumar, S., Aaron, J., and Sokolov, K. V. (2008) Directional conjugation of antibodies to nanoparticles for synthesis of multiplexed optical contrast agents with both delivery and targeting moieties. *Nat. Protoc. 3*, 314−320.
(80) Fleminger, G., Hadas, E., Wolf, T., and Solomon, B. (1990) Oriented immobilization of periodate-oxidized monoclonal antibodies on amino and hydrazide derivatives of Eupergit C. *Appl. Biochem. Biotechnol. 23*, 123−37.
(81) Thierry, B., Ng, J., Krieg, T., and Griesser, H. J. (2009) A robust procedure for the functionalization of gold nanorods and noble metal nanoparticles. *Chem. Commun. 0*, 1724−1726.
(82) Beamson, G., and Briggs, D. (1992) *High resolution XPS of organic polymers: the Scienta ESCA300 database*, Wiley, Chichester [England]; New York.
(83) Perry, J. L., Reuter, K. G., Kai, M. P., Herlihy, K. P., Jones, S. W., Luft, J. C., Napier, M., Bear, J. E., and DeSimone, J. M. (2012) PEGylated PRINT nanoparticles: the impact of PEG density on protein binding, macrophage association, biodistribution, and pharmacokinetics. *Nano Lett. 12*, 5304−5310.

(84) Vigderman, L., Manna, P., and Zubarev, E. R. (2012) Quantitative replacement of cetyl trimethylammonium bromide by cationic thiol ligands on the surface of gold nanorods and their extremely large uptake by cancer cells. *Angew. Chem., Int. Ed. 51*, 636−641.
(85) Chanda, N., Shukla, R., Katti, K. V., and Kannan, R. (2009) Gastrin releasing protein receptor specific gold nanorods: breast and prostate tumor avid nanovectors for molecular imaging. *Nano Lett. 9*, 1798−1805.
(86) Liz-Marzán, L. M., Pérez-Juste, J., and Pastoriza-Santos, I. (2008) Plasmonics of Gold Nanorods. Considerations for Biosensing, in *Nanomaterials for Application in Medicine and Biology* (Giersig, M., and Khomutov, G. B., Eds.) pp 103−111, Springer, Netherlands.
(87) Wang, X., Li, Y., Wang, H., Fu, Q., Peng, J., Wang, Y., Du, J., Zhou, Y., and Zhan, L. (2010) Gold nanorod-based localized surface plasmon resonance biosensor for sensitive detection of hepatitis B virus in buffer, blood serum and plasma. *Biosens. Bioelectron. 26*, 404−410.
(88) Alkilany, A. M., Nagaria, P. K., Hexel, C. R., Shaw, T. J., Murphy, C. J., and Wyatt, M. D. (2009) Cellular uptake and cytotoxicity of gold nanorods: molecular origin of cytotoxicity and surface effects. *Small 5*, 701−708.
(89) Alkilany, A. M., Nagaria, P. K., Wyatt, M. D., and Murphy, C. J. (2010) Cation exchange on the surface of gold nanorods with a polymerizable surfactant: polymerization, stability, and toxicity evaluation. *Langmuir 26*, 9328−9333.
(90) Aaron, J., Travis, K., Harrison, N., and Sokolov, K. (2009) Dynamic imaging of molecular assemblies in live cells based on nanoparticle plasmon resonance coupling. *Nano Lett. 9*, 3612−3618.